Vortex Wavefront FMCW ISAC Model: A Blender-Based Evaluation

Yuan Liu[1], Wen-Xuan Long[2,3], Rui Chen[2], Linlong Wu[1], M. R. Bhavani Shankar[1]
[1]Interdisciplinary Centre for Security, Reliability and Trust (SnT), University of Luxembourg, L-1855, Luxembourg
[2]State Key Laboratory of Integrated Service Networks (ISN), Xidian University, Shaanxi, China
[3]Dipartimento di Ingegneria dell'Informazione, University of Pisa, Italy

***Abstract*—Integrated sensing and Communication (ISAC) systems are key enablers for 6G networks, offering promising applications in indoor scenarios, such as high-accuracy localization, tracking, imaging, augmented senses, and gesture recognition. In this paper, we propose a radar-centric ISAC model based on frequency-modulated continuous-wave (FMCW) waveform, where a unified circular array (UCA) is employed to generate the vortex electromagnetic (EM) waves with the helical wavefront. Benefiting from the additional angular diversity provided by this wavefront, the proposed model can achieve a high-resolution angle estimation and avoid performance ambiguities due to multiple-inputs and multiple-outputs (MIMO) multiplexing. For validation, a Blender-based ray tracing simulator is utilized to acquire realistic channel data of indoor environments. Comparisons of the proposed ISAC model and the conventional FMCW MIMO radar are given under the indoor scenario. Our evaluation accounts for multiple target estimations and illustrates a trade-off between radar properties and communication spectral efficiency. This analysis provides valuable insights for optimizing ISAC systems in future 6G networks.**

***Index Terms*—Blender, FMCW, ISAC, OAM, vortex wavefront**

I. Introduction

Recently, the design of integrated sensing and communication (ISAC) systems at millimeter wave (mmWave) band becomes a focus. The main reasons are twofold [1], [2]. First, mmWave becomes an important frequency band for both high-resolution sensors and next-generation communications. The necessity of spectrum sharing motivates ISAC system studies. Second, some industrial-driven applications require both communications and sensing at the terminals, e.g., autonomous driving, indoor robots, and industrial Internet of Things (IIoTs).

The existing ISAC systems can be communication-centric, radar-centric, and joint design schemes. In this context, this paper concentrates on radar-centric performance design. This approach is pursued since, for some indoor applications, the need for high-resolution range-angle-Doppler estimation is even higher than the state-of-the-art, while the current communication rates are sufficient for non-video transmissions. For example, the high-accuracy localization and tracking, simultaneous localization, imaging, and mapping (SLIAM), augmented human sense, gesture and activity recognition [3].

Multiple inputs and multiple outputs (MIMO) radars enable angle estimation and a large number of antennas are required for high-resolution angular estimation. However, orthogonal waveforms enabled by time division multiplexing (TDM), code division multiplexing (CDM), or frequency division multiplexing (FDM) are needed to separate the signals transmitted by different Txs [4]. Using orthogonal waveforms for a large number of antennas can result in ambiguities of other radar performances. Consider the M Txs radar array as an example, the pulse recurrence interval (PRI) increases to M times for both TDM and binary phase multiplexing (BPM)-MIMO, which will result in Doppler velocity ambiguity. It is a classical angle-Doppler trade-off in MIMO radars.

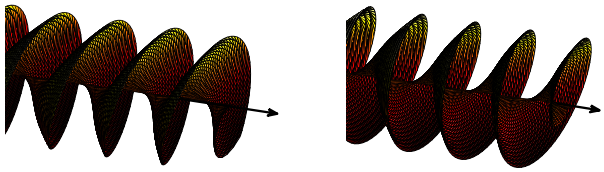

(a) (b)

Figure 1: The vortex wavefront of an OAM beam with mode number: (a) $\ell_u = +1$, (b) $\ell_u = -1$.

A potential solution is to introduce vortex electromagnetic (EM) waves into the existing MIMO radar [5]. The wavefront of vortex EM waves can carry orbital angular momentum (OAM) rotating in azimuth axis, and form a helical structure $e^{j\ell_u\varphi}$ in space, as shown in Fig. 1. Here φ represents transverse azimuth angle, and ℓ_u is an integer known as the OAM mode number [6]. This vortex wavefront can be considered as a composition at the target of multiple plane waves with spatial modulation in azimuth angles. Hence, it can achieve continuous sampling in a three-dimensional space. The vortex wavefront MIMO radar is expected to have a high-angle resolution beyond the limit of the MIMO orthogonal multiplexing waveform and antenna aperture.

In this paper, we propose a radar-centric frequency-modulated continuous-wave (FMCW) waveform ISAC model based on a unified circular array (UCA). This model utilizes the spatial information provided by the EM vortex to detect the high-resolution azimuth-elevation angles and avoids traditional MIMO radar ambiguity. For communication functions,

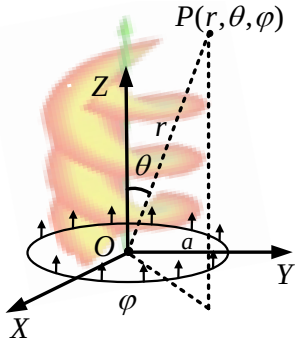

Figure 2: Coordinate of UCA transmitter.

phase modulation (PM), and frequency modulation (FM) are all embedded into the FMCW waveform, hence it provides good communication rates. Besides, we utilize a realistic environment-based radar simulator to analyze the radar-centric performance, where the range-elevation-azimuth images are presented.

II. A Novel ISAC Model Based on Vortex Wavefront FMWC Waveform

A. UCA-based EM vortex wavefront

The UCA shown in Fig 2 is a simple way to generate vortex EM waves [7]. The N antennas are located along the perimeter of a circle, with the spherical coordinates of the nth antenna being $(R, 0, \phi_n)$, where R is the radius of the circle and $\phi_n = 2\pi(n-1)/N$. For an arbitrary point $P(r,\theta,\varphi)$ in the far field, the electric field vector $\boldsymbol{E}_n(r,\theta,\varphi)$ generated by the nth antenna takes the form as [8], [9]

$$\begin{aligned}\boldsymbol{E}_n(r,\theta,\varphi) &= \beta \int |\boldsymbol{r}-\boldsymbol{r}_n|^{-1} e^{jk|\boldsymbol{r}-\boldsymbol{r}_n|} dV_n \\ &\approx \beta \cdot \frac{e^{jkr}}{r} e^{-j\boldsymbol{k}\cdot\boldsymbol{r}_n} \end{aligned} \tag{1}$$

where β models all the constants relative to each transmit antenna element, $\boldsymbol{r}$ is the position vector of P, j is the unit of the complex number, and k is the wave number, $\int(\cdot)dV_n$ is integral for the dipole in the element n.

To generate the vortex wave with mode ℓ_u, the N elements in the UCA transmit the same input signal with a successive phase-shift $\ell_u\phi_n$ to the nth element. Thus, at the point $P(r,\theta,\varphi)$, the electric field vector $\boldsymbol{E}_t(r,\theta,\varphi)$ generated by the superposition of N elements is given by [8], [9]

$$\begin{aligned}\boldsymbol{E}_t(r,\theta,\varphi) &= \beta \frac{e^{jkr}}{r} \sum_{n=0}^{N-1} e^{-j(\boldsymbol{k}\cdot\boldsymbol{r}_n - \ell_u\phi_n)} \\ &\approx \beta \frac{e^{jkr} N e^{j\ell_u\varphi}}{4\pi r} j^{-\ell_u} J_\ell(kR\sin\theta), \end{aligned} \tag{2}$$

where $J_{\ell_u}(kR\sin\theta) = \frac{j^{\ell_u}}{2\pi}\int_0^{2\pi} e^{-jkR\sin\theta\cos\phi'} e^{-j\ell_u\phi'}$ is the first kind of ℓ_uth-order Bessel function and $\phi' = \varphi - \phi_n$.

B. Communication symbols-embedded FMCW

FMCW is widely used in radar systems, due to the low-cost and efficient de-chirp techniques. The transmitter (Tx) transmits linear frequency-modulated chirps sequentially, with each coherent processing interval (CPI) consisting of L chirps. Assuming to transmit a unit power, the transmitted lth chirp can be represented as

$$s(t;l) = e^{j2\pi(f_l + \frac{1}{2}\mu(t-(l-1)T_c))(t-(l-1)T_c)}, \tag{3}$$

where, $l = 1, 2, ..., L$ denotes the chirp index, f_l is the carrier frequency, slope $\mu = B/T_c$, B represents the bandwidth, and T_c is the chirp duration. Those parameters limit the radar performances, e.g., the range resolution is

$$\Delta R = \frac{c}{2B}, \tag{4}$$

where c is the speed of light.

There are several approaches to embedding communication symbols into FMCW chirp, i.e., amplitude modulation (AM), PM, and FM [10], [11].

To increase the communication rates, one FMCW chirp can be split into $D = 2^M$ sub-chirps, with M being a positive integer. The starting frequency of each sub-chirp can be modulated by the FM symbol $\alpha_{l_d}^{\text{FM}} \in [0, 2^M - 1]$ as $f_l + \alpha_{l_d}^{\text{FM}} B'$. Each sub-chirp can be modulated with the PM symbol $\alpha_{l_d}^{\text{PM}}$. The sensing and communication model of the dth sub-chirp of the lth chirp (denoted as l_d, $l_d = (l-1)D + d - 1$) is

$$s_{\text{SC}}(t;l_d) = \mathbf{s}_b(t;l_d) e^{j2\pi f_l}, \tag{5}$$

where the baseband signal

$$s_b(t;l_d) = e^{j\alpha_{l_d}^{\text{PM}}} e^{j2\pi(\alpha_{l_d}^{\text{FM}} B' + \frac{1}{2}\mu(t-(l-1)T_c))(t-(l_d-1)T_0)}. \tag{6}$$

where the bandwidth and duration of one sub-chirp are $B' = B/D$ and $T_0 = T_c/D$, respectively.

Assuming that the constellation size of PM is A_{PM}. By applying the sub-chirp strategy, the transmission rate C_{rate} is increased with D as

$$C_{\text{rate}} = \frac{D}{T_c}(\log_2 D + \log_2 A_{\text{PM}}), \tag{7}$$

However, due to the application of utilizing the sub-chirps, the range resolution in (4) fades to

$$\Delta R' = \frac{c}{2B'} = \Delta R D. \tag{8}$$

Hence, there has a trade-off between the range resolution and communication rates, which can be balanced through a reasonable design of D.

C. UCA-aided ISAC model

In conventional FMCW in (3), L chirps consist of one CPI in radar. Using the sub-chirp FMCW model in (6), one CPI consists of LDth sub-chirps. Then, the baseband signals are transmitted by the UCA shown in Fig. 2 with a successive phase-shift $\{\ell_{u,d}\phi_n | n = 0, 1, \cdots, N-1; \ell_{u,d} = -(N-1)/2, -(N-1)/2+1, ..., (N-1)/2\}$. As $LD \gg (N-1)/2$, in the l_dth sub-chirp, $\ell_{u,d} = l_d \mod (N-1)$.

For an arbitrary point $P(r,\theta,\varphi)$ in the far field, the signal model generated by the superposition of N elements with added phase shifts is given by

$$r_P(t;l_d)=\sum_{n=1}^{N}h_p\mathbf{s}_{\mathrm{b}}(t-\tau_p;l_d)e^{j\ell_{u,d}\phi_n}e^{j2\pi f_l}, \tag{9}$$

h_p denotes the propagating attenuation from the antennas to the position P, τ_p is the propagating delay. Applying the transform in (2), we obtain

$$\begin{aligned}&r_P(t;l_d)\\&=j^{-l_d}h_pNs_{\mathrm{b}}(t-\tau_p;l_d)e^{\ell_{u,d}\varphi}J_{\ell_{u,d}}(kR\sin\theta)e^{j2\pi f_l}.\end{aligned} \tag{10}$$

By using a UCA and applying the phase-shift $\ell_{u,d}\phi_n$ to the nth antenna, we generate the vortex wavefront at the far field. Here we can observe that both the azimuth and elevation angles are coupled.

III. The de-chirp and demodulation of the dual functions

We assume that the dual-function Tx and radar receiver (Rx) are co-located and have the same radius, while the communication Rx is separated.

A. The de-chirp of radar function

The received radar signal is the superposition of the N antennas without additional phase shift, i.e., it can be equivalent to a zero-order Bessel function. Considering Q targets, and the position of the qth target is $q(r_q,\theta_q,\varphi_q)$. The received echo radar function is

$$\begin{aligned}r_{\mathrm{rad}}(t;l_d)=&\sum_{q=1}^{Q}j^{-l_d}N^2h_q^2\sigma_q s_{\mathrm{b}}(t-\tau_q;l_d)e^{j2\pi f_l}\\&e^{j\ell_{u,d}\varphi_q}J_{\ell_{u,d}}(kR\sin\theta_q)J_0(kR\sin\theta_q)\end{aligned} \tag{11}$$

where h_q is the propagation fading between the qth target and the radar, σ_q is the radar cross section (RCS), τ_q is the propagation delay as

$$\tau_q=2\frac{r_q+v_q(l_d-1)T_0}{c}=2\frac{\tilde{r_q}}{c}, \tag{12}$$

where v_q is the speed of the qth target, r_q is the range between the qth target. The modulated communication symbols are known on the radar Rx side, then the intermediate frequency (IF) signal can be calculated as

$$r_{\mathrm{IF}}(t;l_d)=r_{\mathrm{rad}}(t;l_d)e^{-j2\pi\alpha_{l_d}^{\mathrm{PM}}}e^{-j2\pi(f_l+\alpha_{l_d}^{\mathrm{FM}}B_0+\frac{1}{2}\mu t)t}. \tag{13}$$

The sampled IF signal as a function of fast time and slow time is

$$\begin{aligned}\mathbf{Z}(n_s;l_d)=&j^{-l_d}N^2\sum_{q=1}^{Q}h_q^2\sigma_q e^{j2\pi\frac{2\mu\tilde{r_q}}{c}\frac{n_s-1}{F_s}}\\&e^{j\ell_{u,d}\varphi_q}J_{\ell_{u,d}}(k_sa\sin\theta_q)J_0(k_sa\sin\theta_q),\end{aligned} \tag{14}$$

where

$$k_s=\frac{2\pi\mu(n_s-1)}{cF_s}, \tag{15}$$

where $n_s=1,2,...,N_s/D$ is the index of fast time with N_s is the number samples in one complete FMCW chirp, F_s is the sampling frequency.

In (14), the azimuth angle φ_q is coupled with the OAM mode number $\ell_{u,d}$, the $r_q(t)$ is coupled with k_s, and the elevation angle θ_q is coupled with both $\ell_{u,d}$ and k_s in the Bessel function. We can apply the recursive MUSIC algorithm in [9] to do the parameter estimations. By doing the recursive MUSIC algorithm in the OAM mode domain, we can estimate the $\{(\theta_q,\varphi_q)\}$, i.e., the azimuth-elevation angle map. By doing the recursive MUSIC algorithm in the OAM mode domain, we can estimate $\{(\tilde{r_q},\theta_q)\}$, i.e., range-angle map. Eventually, the estimates of $\{(\theta_q,\varphi_q)\}$ can be combined with the estimates of $\{(\tilde{r_q},\theta_q)\}$ to estimate the 3-D position of all the scattering points.

By using the OAM-aided FMCW waveform, we could estimate both the azimuth and elevation angles, while avoiding using the orthogonal multiplexing waveforms in conventional FMCW MIMO radar.

B. The demodulation of communication function

Considering the single antenna communication Rx located at $(r^{q_c},\theta^{q_c},\varphi^{q_c})$. The received signal at the communication Rx side can be:

$$r_{\mathrm{com}}(t;l_d)=\sum_{n=1}^{N}h_n^{q_c}s_b(t-\tau_{q_c};l_d)e^{jl_d\phi_n}e^{j2\pi f_l}+n(t), \tag{16}$$

where $h_n^{q_c}$ is the channel attenuation between the nth Tx to the communication Rx, τ_{q_c} is the delay, $n(t)$ is additive white Gaussian noise (AWGN). It is worth mentioning that, $h_n^{q_c}$ is a function of frequency, here for simplification, we assume it is a constant during one sub-chirp.

The demodulation of FM symbols is required to obtain the correct down-converted signal. Hence, we demodulate the FM signal first. Applying the energy indicator method in [11], and using $\hat{\alpha}_{l_d}^{\mathrm{FM}}$ to represent the estimated FM symbol. The down-converted signal $y_{\mathrm{com}}(t;l_d)=r_{\mathrm{com}}(t;l_d)e^{-j2\pi(f_l+\hat{\alpha}_{l_d}^{\mathrm{FM}}B_0+\frac{1}{2}\mu t)t}$ can be simplified as

$$\begin{cases}\sum_{n=1}^{N}h_n^{q_c}e^{j\alpha_{l_d}^{\mathrm{PM}}}e^{jl_d\phi_n}e^{\phi(\tau_{q_c})}+\hat{n}(t),\hat{\alpha}_{l_d}^{\mathrm{FM}}=\alpha_{l_d}^{\mathrm{FM}},\\\sum_{n=1}^{N}h_n^{q_c}e^{j\alpha_{l_d}^{\mathrm{PM}}}e^{j2\pi(f_l+(\hat{\alpha}_{l_d}^{\mathrm{FM}}-\alpha_{l_d}^{\mathrm{FM}})B_0+\frac{1}{2}\mu(t-\tau_{q_c}))(t-\tau_{q_c})}+\hat{n}(t),\\\quad\hat{\alpha}_{l_d}^{\mathrm{FM}}\neq\alpha_{l_d}^{\mathrm{FM}},\end{cases} \tag{17}$$

where, $\phi(\tau_{q_c})$ is a constant phase related to τ_{q_c}. The equation under the condition of $\hat{\alpha}_{l_d}^{\mathrm{FM}}\neq\alpha_{l_d}^{\mathrm{FM}}$ can be filtered out by the low pass filter (LPF). Then, sampling the $y_{\mathrm{com}}(t;l_d)$ at the radar process F_s, we obtain discredited $\mathbf{y}_{\mathrm{com}}(n_s;l_d)$. In a full FMCW chirp, the sampling number is N_s, for each sub-chirp, the sampling number is N_s/D, thus $\mathbf{y}_{\mathrm{com}}(n_s;l_d)\in\mathbb{C}^{N_s/D\times1}$. Then

$$\hat{\alpha}_{l_d}^{\mathrm{FM}}=\arg\max_{\hat{\alpha}_{l_d}^{\mathrm{FM}}\in[0,1,...,2^M-1]}E(\hat{\alpha}_{l_d}^{\mathrm{FM}}), \tag{18}$$

where

$$E(\hat{\alpha}_{l_d}^{\mathrm{FM}}) = \left| \frac{D}{N_s} \sum_{n_s=1}^{N_s/D} \mathbf{y}_{\mathrm{com}}(n_s; l_d) \right|^2. \tag{19}$$

Now that we have obtained the correct $\alpha_{l_d}^{\mathrm{FM}}$, i.e., the received discrete baseband signal $\mathbf{y}_{\mathrm{com}}(n_s; l_d)$. The next step is to do demodulation of PM.

Assuming that we have perfect channel estimation $\hat{\mathbf{h}}_c^{q_c} \mathbb{C}^{N_s/D \times 1}$, the physical channel can be estimated together with the vortex phase shift as

$$\hat{\mathbf{h}}_c^{q_c}(n_s) = \sum_{n=1}^{N} h_n^{q_c} e^{-j2\pi \mathbf{f}_c(n_s)(r^{q_c} - \phi_{\mathrm{UCA}}^{q_c})/c} e^{jl_d\phi_n}. \tag{20}$$

where

$$\mathbf{f}_c(n_s) = e^{f_l + \hat{\alpha}_{l_d}^{\mathrm{FM}} B_0 + \frac{n_s}{2F_s}\mu}, \tag{21}$$

and the delay due to the UCA array [12]

$$\phi_{\mathrm{UCA}}^{q_c} = R \sin\theta^{q_c} \cos(\varphi^{q_c} + \varphi_n). \tag{22}$$

The $\alpha_{l_d}^{\mathrm{PM}}$ can be estimated through maximum likelihood as

$$\hat{\alpha}_{l_d}^{\mathrm{PM}} = \arg\min_{\hat{\alpha}_{l_d}^{\mathrm{PM}}} \left| \frac{D}{N_s} \sum_{n_s=1}^{N_s/D} \left(\mathbf{y}_{\mathrm{com}}(n_s; l_d) - e^{j\hat{\alpha}_{l_d}^{\mathrm{PM}}} \hat{\mathbf{h}}_c^{q_c}(n_s) \right) \right|. \tag{23}$$

In this scheme, the communication symbols of the vortex wavefront FMCW model are demodulated. It is worth mentioning that, in this paper, the vortex wavefront is only used for angle estimations of radar functions. In future work, the orthogonality between different OAM modes can be used to increase communication rates.

IV. Blender-Based Scenario Evaluation

In this section, we investigate the potential of the vortex wavefront FMCW model in a relatively realistic indoor scenario. We use a developing Blender-based channel simulator in our group to do the environment-based simulation. Blender is an open-source animation tool that is used for environment modeling [13]. Using the ray tracing engine embedded, it can render the propagation paths in the simulated environment. The tool is flexible to define the material properties, geometry size, and moving trajectories of the objects, hence providing a realistic channel. More information about the simulator can be found in the application case [14].

A. Sensing simulation: range, azimuth, and elevations

The simulation scenario is shown in Fig. 3. In Fig. 3 (a), the distances, azimuth angles, and elevation angles of the two targets can be observed. In Fig. 3 (b), the channel impulse response (CIR) is presented and the ranges of the two targets can be observed. The simulated radar configurations are in Table. I.

We compare the traditional FFT-based estimation results in TDM MIMO radar with the recursive MUSIC estimation results in the proposed model in Fig. 4 and Fig. 5. From

Table I: Radar configurations

Configurations	Values
Central frequency f_c [GHz]	77
Bandwidth B [GHz]	1.8
FMCW slope β [MHz/μs]	30
pulse repetition interval T_{c} [μs]	60
pulse repetition count K	128
Sampling rates f_s [MHz]	10
Fast time sampling number N_s	256
Number of UCA elements	32
Number of ULA	8×4

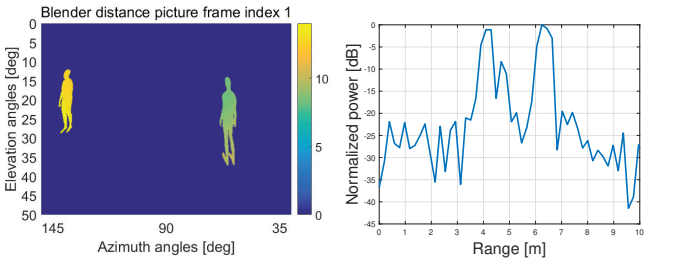

(a) Rendered scenario

(b) Simulated channel pulse response with 20 dB SNR

Figure 3: Scenario and channel: in (a), the x-axis and y-axis denote the exact azimuth and elevation angles, and the color denotes the round distances between the targets and radar; in (b), the power shown are normalized.

the results of these figures, we can easily observe that both methods can identify the two targets and estimate the positions of the two indoor persons.

However, the recursive MUSIC estimation has a higher angle resolution than the traditional FFT-based estimation. Besides, for both the elevation and azimuth estimation, the recursive MUSIC-based circular model provides a similar angle resolution. For the conventional FFT-based MIMO model, the resolution depends on the number of antennas. In Fig. 5, the angle resolution of azimuth is almost two times of elevation, because we use 8 antennas in the azimuth direction and 4 antennas in the elevation direction. Moreover, as we discussed in (14), by doing the recursive MUSIC algorithm in the OAM mode domain, we can estimate directly the azimuth-elevation map rather than combing the rang-azimuth map and rang-Doppler in the FFT-based estimation.

B. Communication simulation:

Based on (7) and (8), we compare the impact of the number of sub-chirps $D = 2^M$, i.e., the FM constellation size, the range resolution, and transmission rate, as shown in Fig. 6. When $D = 1$, the range resolution is $0.83\ m$ according to (8), i.e., the $1/\Delta R = 12\ m^{-1}$. As the number of sub-chirp D increases, the range resolution deteriorates, however, the transmission rate increases with D. Hence, a reasonable D can achieve a balance between the range resolution and transmission rate. It also can be observed that the communication rates increase with the constellation size of PM.

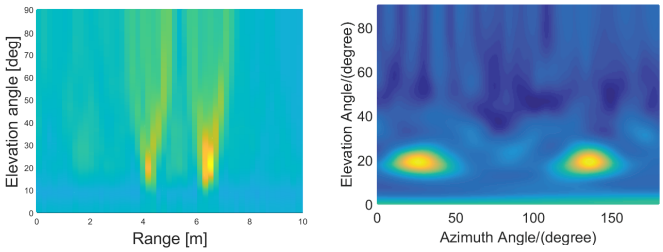

(a) Range-elevation angle (b) Azimuth-elevation angle

Figure 4: Recursive MUSIC estimation results with vortex EM waves.

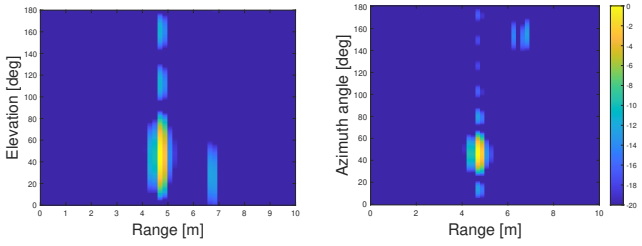

(a) Range-elevation angle (b) Range-azimuth angle

Figure 5: FFT estimation results with TDM MIMO.

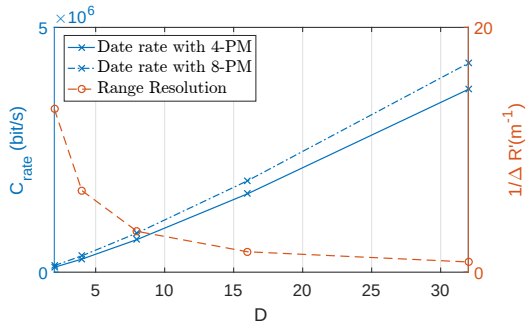

Figure 6: The range resolution and data rate versus the number of sub-chirp D.

V. Conclusion

In this paper, we propose a radar-centric FMCW ISAC model, in which a UCA is employed to generate the vortex wavefront. This spatial modulation provides an additional dimension for angle estimation. The Blender-based ray tracing simulator is utilized to evaluate the proposed ISAC model and compared them with conventional FMCW MIMO radar. Evaluation results show that due to angular diversity provided by vortex EM waves, the proposed model achieves higher angle resolution and avoids radar performance ambiguities of orthogonal MIMO waveforms. Furthermore, we showed the trade-off between radar range resolution and communication data rate by designing the number of sub-chirps reasonably.

Acknowledgment

This work was supported in part by the Luxembourg National Research Fund (FNR) through the BRIDGES project MASTERS under grant BRIDGES2020/IS/15407066 and the CORE project SPRINGER under Grant C18/IS/12734677, in part by the National Natural Science Foundation of China under Grant 62271376, and in part by the Guangdong Natural Science Fund for Distinguished Young Scholar under Grant 2023B1515020079.

References

[1] K. V. Mishra, M. Bhavani Shankar, V. Koivunen, B. Ottersten, and S. A. Vorobyov, "Toward Millimeter-Wave Joint Radar Communications: A Signal Processing Perspective," *IEEE Signal Processing Magazine*, vol. 36, no. 5, pp. 100–114, 2019.

[2] S. H. Dokhanchi, B. S. Mysore, K. V. Mishra, and B. Ottersten, "A mmWave Automotive Joint Radar-Communications System," *IEEE Transactions on Aerospace and Electronic Systems*, vol. 55, no. 3, pp. 1241–1260, 2019.

[3] D. K. Pin Tan, J. He, Y. Li, A. Bayesteh, Y. Chen, P. Zhu, and W. Tong, "Integrated Sensing and Communication in 6G: Motivations, Use Cases, Requirements, Challenges and Future Directions," in *2021 1st IEEE International Online Symposium on Joint Communications & Sensing (JC&S)*, 2021, pp. 1–6.

[4] H. Sun, F. Brigui, and M. Lesturgie, "Analysis and comparison of MIMO radar waveforms," in *2014 International Radar Conference*, 2014, pp. 1–6.

[5] K. Liu, Y. Cheng, X. Li, and Y. Gao, "Microwave-Sensing Technology Using Orbital Angular Momentum: Overview of Its Advantages," *IEEE Veh. Technol. Mag.*, vol. 14, no. 2, pp. 112–118, Jun. 2019.

[6] L. Allen, M. W. Beijersbergen, R. Spreeuw, and et al., "Orbital angular momentum of light and the transformation of Laguerre-Gaussian laser modes," *Phys. Rev. A*, vol. 45, no. 11, pp. 8185–8189, Jul. 1992.

[7] R. Chen, W. X. Long, X. Wang, and L. Jiandong, "Multi-mode oam radio waves: Generation, angle of arrival estimation and reception with UCAs," *IEEE Trans. Wireless Commun.*, vol. 19, no. 10, pp. 6932–6947, Oct. 2020.

[8] R. Chen, W.-X. Long, Y. Gao, and J. Li, "Orbital angular momentum-based two-dimensional super-resolution targets imaging," in *Proc. IEEE Global Conf. Signal Inf. Process.*, 2018, pp. 1–4.

[9] W.-X. Long, R. Chen, M. Moretti, W. Zhang, and J. Li, "Joint OAM Radar-Communication Systems: Target Recognition and Beam Optimization," *IEEE Transactions on Wireless Communications*, pp. 1–1, 2022.

[10] D. Ma, N. Shlezinger, T. Huang, Y. Liu, and Y. C. Eldar, "FRaC: FMCW-Based Joint Radar-Communications System Via Index Modulation," *IEEE Journal of Selected Topics in Signal Processing*, vol. 15, no. 6, pp. 1348–1364, 2021.

[11] M.-X. Gu, M.-C. Lee, Y.-S. Liu, and T.-S. Lee, "Design and Analysis of Frequency Hopping-Aided FMCW-Based Integrated Radar and Communication Systems," *IEEE Transactions on Communications*, vol. 70, no. 12, pp. 8416–8432, 2022.

[12] O. Edfors and A. J. Johansson, "Is Orbital Angular Momentum (OAM) Based Radio Communication an Unexploited Area?" *IEEE Transactions on Antennas and Propagation*, vol. 60, no. 2, pp. 1126–1131, 2012.

[13] B. Foundation. Blender is the free and open source 3D creation suite. [Online]. Available: https://www.blender.org/

[14] Y. Liu, M. Ahmadi, J. Fuchs, and M. R. B. Shankar, "Time-Code-Spatial Modulated IRS-Aided Radar Localization in NLoS Scenario," in *2023 IEEE Radar Conference (RadarConf23)*, 2023, pp. 1–5.